Available online at www.sciencedirect.com
ScienceDirect
Trans. Nonferrous Met. Soc. China 32(2022) 1178−1187
Transactions of Nonferrous Metals Society of China
www.tnmsc.cn

Phase equilibria in Ni−Ti−Ta ternary system

Cui-ping WANG[1], Peng YANG[1], Yu-hui LIANG[1], Shui-yuan YANG[1], Jia-jia HAN[1], Yong LU[1], Xing-jun LIU[1,2,3]

1. Fujian Provincial Key Laboratory of Materials Genome, College of Materials, Xiamen University, Xiamen 361005, China;
2. State Key Laboratory of Advanced Welding and Joining, Harbin Institute of Technology, Harbin 150001, China;
3. Institute of Materials Genome and Big Data, Harbin Institute of Technology, Shenzhen 518055, China

Received 16 February 2021; accepted 26 October 2021

Abstract: Phase diagrams of two isothermal sections of the Ni−Ti−Ta ternary system at 1000 and 1200 °C in a full composition range were determined by X-ray diffraction and electron probe microanalysis. The experimental results indicated a ternary compound τ phase with low solid solubility and composition ranges of (16.3−22.4) at.% Ta, (15.9−24.1) at.% Ti and (58.5−60.0) at.% Ni at 1000 °C. The two terminal solid solutions (bcc-(Ta) and β-Ti) formed a continuous solid solution at 1000 and 1200 °C. A certain amount of Ti can dissolve into Ni−Ta intermetallic compounds near the Ni−Ta side, with the highest value of 21.9 at.% observed in the Ni_2Ta compound at 1000 °C.

Key words: microstructure; Ni−Ti−Ta ternary system; isothermal section phase diagram; electron probe microanalysis

1 Introduction

Nickel-based superalloys have aerospace applications due to their excellent high-temperature properties and oxidation and corrosion resistance in extremely harsh environments [1,2]. However, to meet the high industrial requirements of structural materials used in high-temperature aviation applications, materials with greater mechanical strength and oxidation and corrosion resistances are required. To improve the properties of these alloys, an excellent method is to add alloy refractory elements [3−6]. For example, Ta addition can significantly improve the oxidation and hot-corrosion resistances of nickel-based alloys by forming a stable oxidation layer at elevated temperatures [4,7−9]. Meanwhile, as Ta is a solid-solution strengthening element, alloying with it can also improve the hot-corrosion and oxidation resistances [10,11]. However, topologically close-packed (TCP) phases will degrade the mechanical properties of superalloys with excessive additions of Ti and Ta elements [12,13]. Therefore, it is necessary to investigate a phase diagram of the ternary Ni−Ti−Ta system, not only for future thermodynamics assessment but also for enhancing its potential practical applications.

The Ni−Ti−Ta ternary system consists of three binary subsystems: Ni−Ti, Ni−Ta and Ti−Ta, as illustrated in Fig. 1 [14−16]. The Ni−Ta binary system has been investigated by many researchers [14,17−23]. In 2018, ZHOU et al [14] reviewed the Ni−Ta system, where only four intermetallic compounds of Ni_2Ta, Ni_3Ta, NiTa and $NiTa_2$, and two terminal solid solutions of fcc-(Ni) and bcc-(Ta) coexist. The Ni_8Ta phase was confirmed to be a metastable phase. Additionally, there are two eutectic reactions, three peritectic reactions, a peritectoid reaction and a congruent transformation in this system. Two eutectic reactions: $L \rightleftharpoons Ni_3Ta$ + fcc and $L \rightleftharpoons Ni_2Ta + Ni_6Ta_7$ occur at 1330 and

Corresponding author: Cui-ping WANG, Tel: +86-592-2180606, Fax: +86-592-2187966, E-mail: wangcp@xmu.edu.cn; Xing-jun LIU, E-mail: lxj@xmu.edu.cn
DOI: 10.1016/S1003-6326(22)65865-5

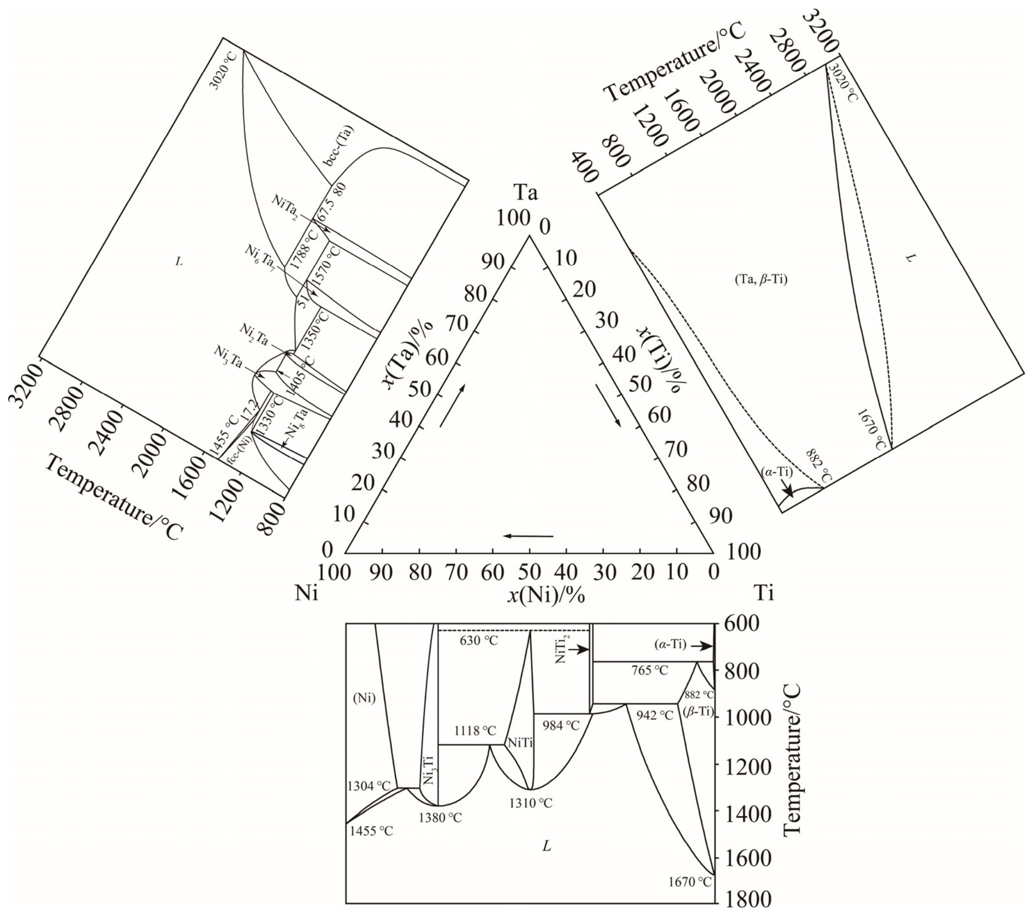

Fig. 1 Binary phase diagrams constituting Ni−Ti−Ta ternary system [14−16]

1350 °C, respectively. The Ni_6Ta_7 and $NiTa_2$ phases form from two peritectic reactions. At present, several investigators have assessed the thermodynamic database of this binary system with the CALPHAD method and first-principles calculations [17−19].

Ni−Ti binary phase diagrams have been reported by many researchers [24−29]. In 2009, KEYZER et al [15] reassessed the Ni−Ti binary phase diagrams and found them to be in good agreement with experimental results. The Ni−Ti binary system contains three intermetallic compounds of Ni_3Ti, NiTi and $NiTi_2$, and three solid solutions of fcc-(Ni), α-Ti and β-Ti. There are three eutectic reactions, one eutectoid reaction and one peritectic reaction in this system. The eutectic transformation of liquid phase (L) occurs at 1304 °C to form fcc-(Ni) and Ni_3Ti; the eutectic transformation of L phase to NiTi and Ni_3Ti occurs at 1118 °C; the eutectic transformation of L phase to $NiTi_2$ and β-Ti occurs at 942 °C. In this study, results of KEYZER et al [15] will be used. The Ti−Ta binary system is homogeneous at high temperatures and a solid solution of α-Ti appears at low temperature [16]. As for the Ni−Ti−Ta ternary system, GUPTA [29] summarized the existing research in 1991, but no information about the phase equilibrium of the Ni−Ti−Ta ternary system was found. In 2007, DU et al [30] investigated the phase equilibria in the Ni−Ti−Ta ternary system at 927 °C. The stable phases in the ternary Ni−Ti−Ta system are listed in Table 1.

In the compositional design and microstructural analysis of nickel-based superalloys, conducting phase equilibrium experiments with the Ni−Ti−Ta ternary system at high temperatures is essential. In the present work, we investigated the phase equilibria of Ni−Ti−Ta systems at 1000 and 1200 °C via electron probe microanalysis (EPMA) and X-ray diffraction (XRD).

2 Experimental

High-purity metals were used as raw materials to prepare the alloys: nickel (99.9 wt.%), titanium (99.9 wt.%) and tantalum (99.9 wt.%). All the

Table 1 Stable solid phases in Ni−Ti−Ta ternary system

System	Phase	Pearson symbol	Prototye	Space group	Strukturbericht	Ref.
Ni−Ta	fcc-(Ni)	*cF*4	Cu	$Fm\overline{3}m$	A1	[14]
	bcc-(Ta)	*cI*2	W	$Im\overline{3}m$	A2	[14]
	Ni_8Ta	*tI*36	Ni_8Nb	*I*4/*mmm*	−	[14]
	Ni_3Ta	*tI*8	$TiAl_3$	*I*4/*mmm*	$D0_{22}$	[14]
	Ni_3Ta	*mP*16	$NbPt_3$	$P2_1/m$	−	[14]
	Ni_3Ta	*oP*8	Cu_3Ti	*Pmmn*	$D0_a$	[14]
	Ni_2Ta	*tI*6	$MoSi_2$	*I*4/*mmm*	$C11_b$	[14]
	Ni_6Ta_7	*hP*13	Fe_7W_6	$R\overline{3}m$	$D8_5$	[14]
	$NiTa_2$	*tI*12	Al_2Cu	*I*4/*mcm*	C16	[14]
Ni−Ti	(Ni)	*cF*4	Cu	$Fm\overline{3}m$	A1	[15]
	α-Ti	*hP2*	Mg	*P*63/*mmc*	A3	[15]
	β-Ti	*cI*2	W	$Im\overline{3}m$	A2	[15]
	Ni_3Ti	*hP*16	Ni_3Ti	*P*63/*mmc*	$D0_{24}$	[15]
	NiTi	*cP*2	CsCl	$Pm\overline{3}m$	B2	[15]
	$NiTi_2$	*cF*96	$NiTi_2$	$Fd\overline{3}m$	$E9_3$	[15]
Ti−Ta	(Ta, *β*-Ti)	*cI*2	W	$Im\overline{3}m$	A2	[16]

metals were well cleared to avoid surface oxidation impurities before melting. All alloys were prepared in the form of molar fractions (at.%). Ingots of around 20 g in mass were re-melted at least five times to obtain uniform alloys with mass loss less than 5% using an arc furnace in a high-purity argon atmosphere with a non-consumable tungsten electrode on a water-cooled copper platform. Then, the samples, except for the liquid phase that precipitated during heat treatment, were individually sealed in high-purity argon quartz tubes and annealed at 1000 and 1200 °C for 30 d. In order to prevent oxidation, some pure yttrium filings were placed in the quartz capsules. Additionally, alloys that precipitated liquid phase during heat treatment were placed separately in an alumina crucible to avoid contact with quartz, and then sealed in a quartz tube with high-purity argon gas. They were annealed at 1000 and 1200 °C for a much shorter duration of 3 h.

All the alloys were water-quenched after heat treatment and well prepared for metallographic analysis. The equilibrium compositions of all phases in the specimens were determined by electron probe microanalysis (EPMA) at an accelerating voltage of 20 kV and a probe current of 1.0×10^{-8} A. The crystal structure was identified by its X-ray diffraction (XRD) pattern using a diffractometer (Phillips Panlytical X-pet) with Cu K_{α} radiation at 40 kV and 40 mA. The results were measured in the 2θ range from 20° to 90° at intervals of 0.015308° and a count time of 0.3 s per step.

3 Results and discussion

3.1 Microstructure

The phase relationship of the Ni−Ti−Ta ternary system at 1000 °C was established based on an analysis of 29 alloys that were annealed for 45 d. The nominal compositions and phase equilibrium compositions of the alloys are displayed in Table 2. Meanwhile, the microstructures and XRD patterns of typical annealed alloys are presented in Figs. 2 and 3, respectively.

Figure 2(a) shows the three-phase equilibrium of NiTi (black) + $NiTa_2$ (grey) + (Ta, *β*-Ti) (white), in the microstructure of the $Ni_{36}Ti_{32}Ta_{32}$ alloy. The corresponding XRD pattern is displayed in Fig. 3(a). Figure 2(b) shows the microstructure of the $Ni_{57}Ti_{21}Ta_{22}$ alloy, which contained three phases: τ (grey) + Ni_6Ta_7 (white) + NiTi (black). In the $Ni_{74}Ti_{10}Ta_{16}$ alloy, a three-phase region of Ni_3Ta (grey) + Ni_2Ta (white) + Ni_3Ti (black) is confirmed

Table 2 Phase equilibrium compositions of phases in Ni−Ti−Ta ternary alloys annealed at 1000 °C

Nominal alloy/at.%	Phase equilibrium			Composition/at.%						Annealing time/d
	Phase 1	Phase 2	Phase 3	Phase 1		Phase 2		Phase 3		
				Ti	Ta	Ti	Ta	Ti	Ta	
$Ni_{17}Ti_{23}Ta_{60}$	Ta, β-Ti	NiTi		9.3	88.7	47.3	4.3			45
$Ni_{39}Ti_{14}Ta_{47}$	Ni_6Ta_7	NiTi	$NiTa_2$	10.7	45.6	41.5	8.8	7.1	57.8	45
$Ni_{56}Ti_{12}Ta_{32}$	Ni_6Ta_7	Ni_2Ta		8.9	40.6	11.7	20.9			45
$Ni_{36}Ti_{32}Ta_{32}$	$NiTa_2$	NiTi	Ta, β-Ti	13.2	51.2	46.4	4.3	8.2	88.2	45
$Ni_{19}Ti_{46}Ta_{35}$	L	Ta, β-Ti		61.6	5.7	31.5	65.5			3/24
$Ni_{57}Ti_{21}Ta_{22}$	Ni_6Ta_7	NiTi	τ	14	36.5	37.8	9.7	20.6	20.1	45
$Ni_{51}Ti_{26}Ta_{23}$	Ni_6Ta_7	NiTi		14.6	37.1	39.3	9.3			45
$Ni_{26}Ti_{53}Ta_{21}$	L	Ta, β-Ti	NiTi	60.2	6.7	30	65.8	53.9	3.2	3/24
$Ni_{81}Ti_6Ta_{13}$	Ni_3Ta	fcc-(Ni)	Ni_3Ti	5	17.4	3.8	8.2	6.3	11.2	45
$Ni_{74}Ti_{10}Ta_{16}$	Ni_3Ta	Ni_2Ta	Ni_3Ti	6.1	17.8	8.7	22.9	14.3	10.3	45
$Ni_{61}Ti_{22}Ta_{17}$	Ni_2Ta	τ	NiTi	16.4	16.3	24.1	16.4	39.4	7	45
$Ni_{55}Ti_{36}Ta_9$	Ni_2Ta	NiTi		18.3	14.9	40.8	6.1			45
$Ni_{86}Ti_8Ta_6$	fcc-(Ni)	Ni_3Ti		6.9	5.1	12	7			45
$Ni_{67}Ti_{26}Ta_7$	Ni_2Ta	Ni_3Ti	NiTi	21.9	11.3	23.5	2.5	41.8	3.5	45
$Ni_{15}Ti_{71}Ta_{14}$	L	Ta, β-Ti		68.5	3.9	73.3	20.4			3/24
$Ni_{91}Ti_1Ta_8$	fcc-(Ni)			1.1	7.7					45
$Ni_{85.5}Ti_{9.5}Ta_5$	fcc-(Ni)	Ni_3Ti		7.5	4	14.5	6.1			45
$Ni_{68}Ti_{25}Ta_7$	Ni_2Ta	Ni_3Ti	NiTi	22.2	11	23.2	2.5	42	3.4	45
$Ni_{61}Ti_{14}Ta_{25}$	Ni_2Ta	τ	Ni_6Ta_7	10.3	22.4	15.9	24.7	9.9	40.1	45
$Ni_{37}Ti_{50}Ta_{13}$	L	Ta, β-Ti	NiTi	60.5	6.5	30.1	66	54.1	3.3	3/24
$Ni_{24}Ti_{63}Ta_{13}$	L	Ta, β-Ti		65.5	5.3	54.4	43.1			3/24
$Ni_{44}Ti_{19}Ta_{37}$	Ni_6Ta_7	NiTi		13.8	41.7	41.7	8.1			45
$Ni_{44}Ti_{16}Ta_{40}$	Ni_6Ta_7	NiTi	$NiTa_2$	14.5	41.3	41.2	9.1	7.5	57.4	45
$Ni_{60}Ti_{13}Ta_{27}$	Ni_2Ta	τ	Ni_6Ta_7	9.5	24	15.9	26.3	9.2	40.5	45
$Ni_{84}Ti_{14}Ta_2$	fcc-(Ni)	Ni_3Ti		10.2	1.1	16.9	3.1			45
$Ni_{63}Ti_{24}Ta_{13}$	Ni_2Ta	NiTi		18.5	14.5	41.7	5.8			45
$Ni_{56}Ti_{31}Ta_{13}$	τ	NiTi		23.5	18	41	7.4			45
$Ni_{41}Ti_{39}Ta_{20}$	Ta, β-Ti	NiTi		9.3	88.7	47.3	4.3			45
$Ni_{32}Ti_{18}Ta_{50}$	$NiTa_2$	NiTi	Ta, β-Ti	13.5	50.8	46.1	4.5	8.5	88	45

in Fig. 2(c). Figure 2(d) features the microstructure of the $Ni_{61}Ti_{22}Ta_{17}$ alloy, which consisted of Ni_2Ta (grey) + NiTi (black) + τ (white), and the XRD analysis in Fig. 3(b) confirms the three-phase microstructure. As described in Fig. 2(e), a two-phase equilibrium of fcc-(Ni) (black) + Ni_3Ti (white) was identified in the $Ni_{86}Ti_8Ta_6$ alloy. The corresponding phase relationship was identified by the XRD results, in which the characteristic peaks of the fcc-(Ni) and Ni_3Ti phases are labelled with different symbols in Fig. 3(c). A three-phase region of Ni_3Ti (black) + NiTi (dark-grey) + Ni_2Ta (white) was found in the $Ni_{68}Ti_{25}Ta_7$ alloy, as shown in Fig. 2(f).

Twenty-three alloys were designed to investigate the phase relation of the Ni−Ti−Ta system at 1200 °C. Table 3 lists the nominal compositions and phase equilibrium compositions

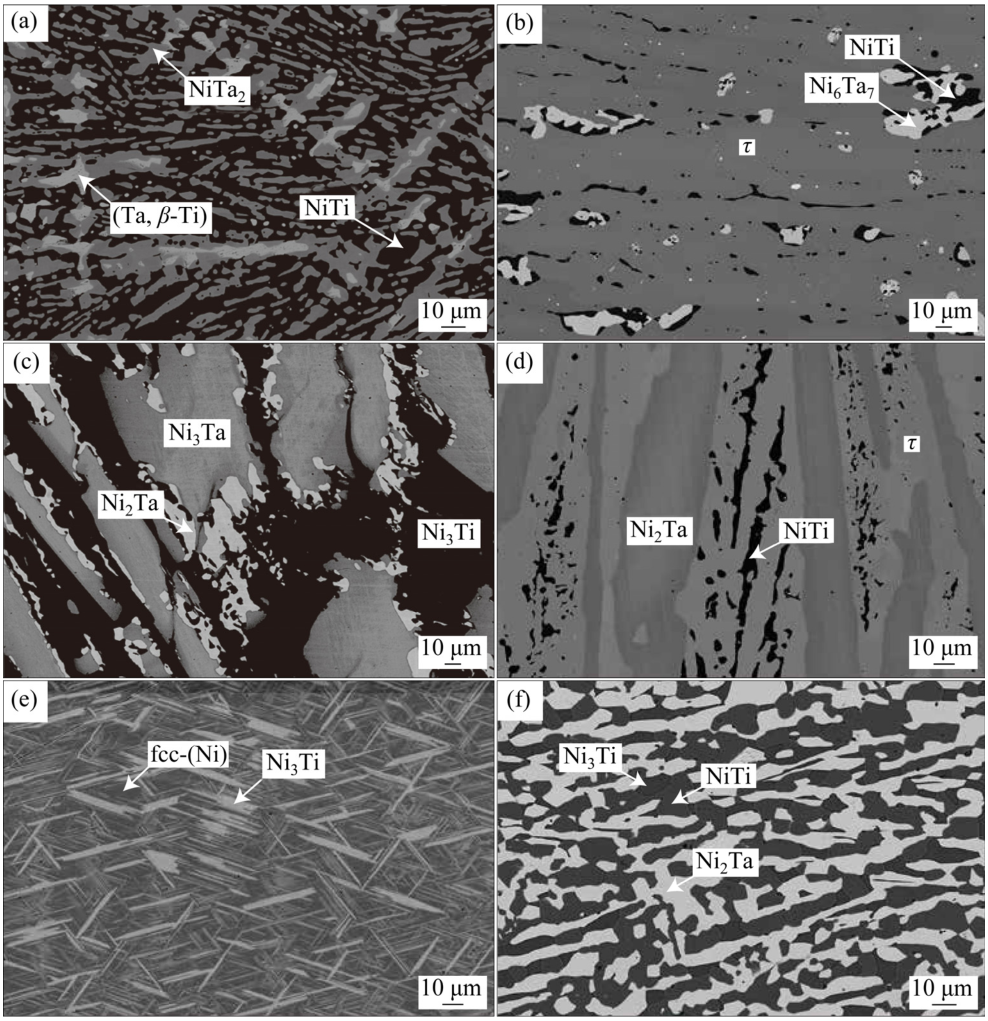

Fig. 2 Microstructures of typical alloys in Ni−Ti−Ta system annealed at 1000 °C for 45 d: (a) $Ni_{36}Ti_{32}Ta_{32}$; (b) $Ni_{57}Ti_{21}Ta_{22}$; (c) $Ni_{74}Ti_{10}Ta_{16}$; (d) $Ni_{61}Ti_{22}Ta_{17}$; (e) $Ni_{86}Ti_{8}Ta_{6}$; (f) $Ni_{68}Ti_{25}Ta_{7}$

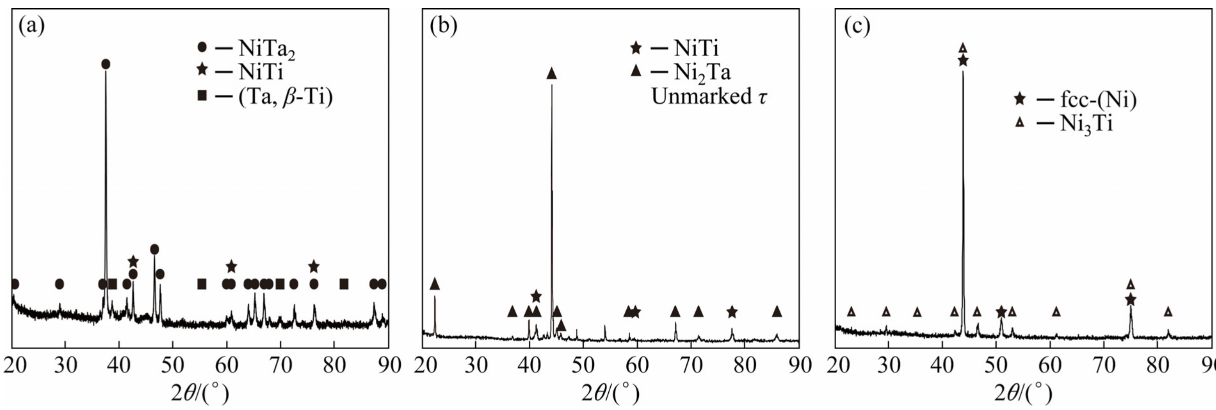

Fig. 3 XRD patterns of typical alloys in Ni−Ti−Ta system annealed at 1000 °C for 45 d: (a) $Ni_{36}Ti_{32}Ta_{32}$; (b) $Ni_{61}Ti_{22}Ta_{17}$; (c) $Ni_{86}Ti_{8}Ta_{6}$

of the alloys. Additionally, the microstructures and XRD patterns of typical alloys are presented in Figs. 4 and 5, respectively. As presented in Fig. 4(a), the microstructure of a three-phase region of $NiTa_2$ (grey) + Ni_6Ta_7 (white) + L (black) was identified in the $Ni_{36}Ti_{32}Ta_{32}$ alloy and the corresponding XRD pattern is displayed in Fig. 5(a). Figure 4(b) shows the two-phase microstructure of L (black) +

Table 3 Phase equilibrium compositions of phases in Ni−Ti−Ta ternary alloys annealed at 1200 °C

Nominal alloy/at.%	Phase equilibrium			Composition/at.%						Annealing time/d
	Phase 1	Phase 2	Phase 3	Phase 1		Phase 2		Phase 3		
				Ti	Ta	Ti	Ta	Ti	Ta	
$Ni_{17}Ti_{23}Ta_{60}$	Ta, β-Ti	L	$NiTa_2$	6.6	92.5	52.2	16.3	9.7	57.1	3/24
$Ni_{39}Ti_{14}Ta_{47}$	Ni_6Ta_7	L	$NiTa_2$	11	46.6	52.2	15.2	5.7	60.7	3/24
$Ni_{56}Ti_{12}Ta_{32}$	Ni_6Ta_7	Ni_2Ta		9.1	42.4	11.3	22.3			30
$Ni_{36}Ti_{32}Ta_{32}$	Ni_6Ta_7	L	$NiTa_2$	10.8	46.2	52	15.3	5.9	60.5	3/24
$Ni_{19}Ti_{46}Ta_{35}$	L	Ta, β-Ti		58.8	7.4	29.3	69.3			3/24
$Ni_{57}Ti_{21}Ta_{22}$	Ni_6Ta_7	τ	L	9.3	40.8	18.4	22	31.8	13.6	3/24
$Ni_{51}Ti_{26}Ta_{23}$	Ni_6Ta_7	L		13.2	40.2	37.3	13.1			3/24
$Ni_{26}Ti_{53}Ta_{21}$	L	Ta, β-Ti		58.2	8.3	28.7	69.9			3/24
$Ni_{81}Ti_6Ta_{13}$	Ni_3Ta	fcc-(Ni)	Ni_3Ti	5.7	17.1	5.8	7.9	8.9	9.5	30
$Ni_{74}Ti_{10}Ta_{16}$	Ni_3Ta	Ni_2Ta	Ni_3Ti	6.7	16.5	13.3	17.6	11	11.5	30
$Ni_{86}Ti_8Ta_6$	fcc-(Ni)	Ni_3Ti		8.4	5.2	12.9	6.5			30
$Ni_{67}Ti_{26}Ta_7$	Ni_2Ta	Ni_3Ti	L	20.1	13.3	21.1	4.4	32.2	4.5	3/24
$Ni_{15}Ti_{71}Ta_{14}$	L	Ta, β-Ti		68.5	3.9	73.3	20.4			3/24
$Ni_{91}Ti_1Ta_8$	fcc-(Ni)			1.1	7.8					30
$Ni_{85.5}Ti_{9.5}Ta_5$	fcc-(Ni)			9.1	4.6					30
$Ni_{68}Ti_{25}Ta_7$	Ni_2Ta	Ni_3Ti	L	20.3	13.1	21	4.6	32.1	4.7	3 h
$Ni_{61}Ti_{14}Ta_{25}$	Ni_2Ta	Ni_6Ta_7		11.4	21.4	9.3	41.4			30
$Ni_{37}Ti_{50}Ta_{13}$	NiTi	L		47.3	4.9	52.3	9.9			3/24
$Ni_{24}Ti_{63}Ta_{13}$	L	Ta, β-Ti		65.5	5.3	54.4	43.1			3/24
$Ni_{60}Ti_{13}Ta_{27}$	Ni_2Ta	Ni_6Ta_7	τ	11	22	9.5	42.4	14.9	24.3	30
$Ni_{84}Ti_{14}Ta_2$	fcc-(Ni)	Ni_3Ti		11.9	2.2	18.7	3.4			30
$Ni_{63}Ti_{24}Ta_{13}$	Ni_2Ta	L		18.2	16.3	31.9	10.1			3/24
$Ni_{41}Ti_{39}Ta_{20}$	Ni_6Ta_7	NiTi	L	19.1	39.8	46.1	6	51.8	12.3	3/24

(Ta, β-Ti) (white) in the $Ni_{19}Ti_{46}Ta_{35}$ alloy. Figure 4(c) displays a three-phase section of L (grey) + Ni_6Ta_7 (white) + NiTi (black) in the $Ni_{41}Ti_{39}Ta_{20}$ alloy. The grey area composed of black and white phases in Fig. 4(c) is a liquid phase region at high temperature. However, after quenching, the liquid phase may undergo a phase transition, resulting in a new white phase. As shown in Fig. 4(d), the microstructure of the $Ni_{67}Ti_{26}Ta_7$ alloy was determined as L (black) + Ni_2Ta (white) + Ni_3Ti (grey). In the $Ni_{17}Ti_{23}Ta_{60}$ alloy, a three-phase equilibrium of (Ta, β-Ti) (white) + L (black) + $NiTi_2$ (grey) was identified, as shown in Fig. 4(e). The XRD analysis in Fig. 5(b) supports the microstructure of this alloy. In the $Ni_{81}Ti_6Ta_{13}$ alloy, a three-phase region of Ni_3Ta (white) + Ni_3Ti (grey) + fcc-(Ni) (black) was confirmed in Fig. 4(f) and the corresponding XRD pattern is displayed in Fig. 5(c).

3.2 Isothermal sections

According to the experimental results, the isothermal sections of the Ni−Ti−Ta ternary system at 1000 and 1200 °C were established and shown in Figs. 6 and 7, respectively. At 1000 °C, nine three-phase regions, ((Ta, β-Ti) + $NiTa_2$ + NiTi), (Ni_6Ta_7 + $NiTa_2$ + NiTi), (Ni_6Ta_7 + Ni_2Ta + τ), (Ni_3Ti + Ni_2Ta + Ni_3Ta), (Ni_3Ti + fcc-(Ni) + Ni_3Ta), (Ni_3Ti + Ni_2Ta + NiTi), (τ + Ni_2Ta + NiTi), (Ni_6Ta_7 + NiTi + τ) and ((Ta, β-Ti) + L + NiTi), were experimentally determined, which are marked as triangles with solid lines. There is a three-phase region (Ni_8Ta +

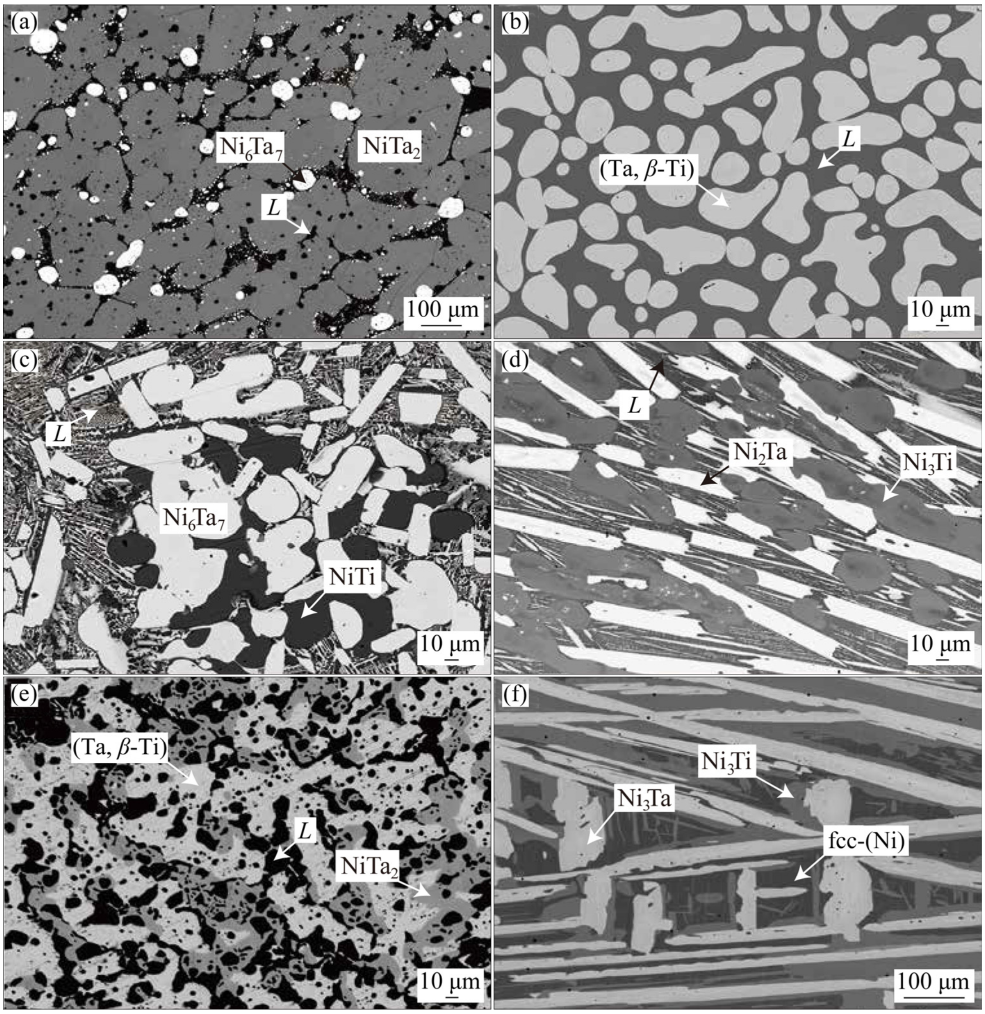

Fig. 4 Microstructures of typical alloys in Ni−Ta−Ti ternary system annealed at 1200 °C for 3 h (a−e) and 30 d (f): (a) $Ni_{36}Ti_{32}Ta_{32}$; (b) $Ni_{19}Ti_{46}Ta_{35}$; (c) $Ni_{41}Ti_{39}Ta_{20}$; (d) $Ni_{67}Ti_{26}Ta_7$; (e) $Ni_{17}Ti_{23}Ta_{60}$; (f) $Ni_{81}Ti_6Ta_{13}$

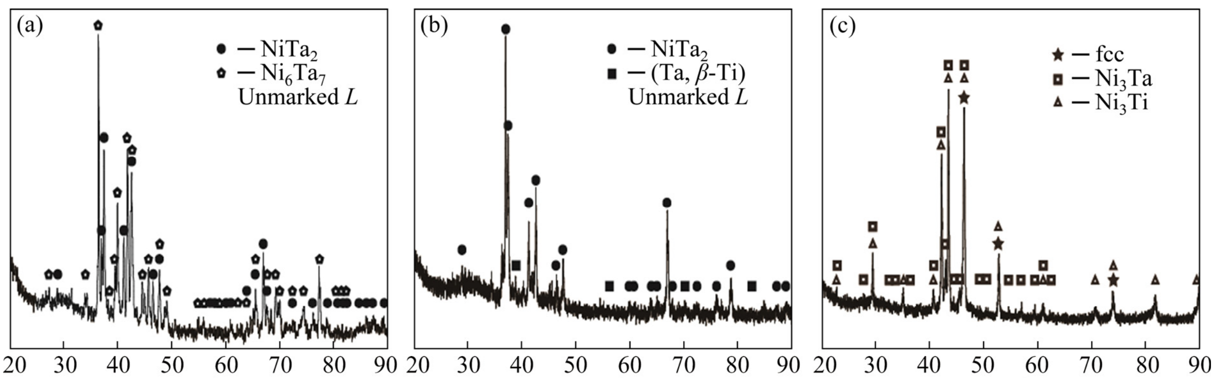

Fig. 5 XRD patterns of typical alloys in Ni−Ta−Ti system annealed at 1200 °C for 3 h (a, b) and 30 d (c): (a) $Ni_{36}Ti_{32}Ta_{32}$; (b) $Ni_{17}Ti_{23}Ta_{60}$; (c) $Ni_{81}Ti_6Ta_{13}$

fcc-(Ni) + Ni_3Ta) that has not been measured experimentally and is represented by a dotted triangle. The corresponding results show that a ternary compound *τ* phase was detected with a small composition range of (58.5−60.0) at.% Ni, (15.9−24.1) at.% Ti and (16.3−22.4) at.% Ta at 1000 °C. Two body centerd cubic terminal solid solutions (Ta) and *β*-Ti formed a continuous phase

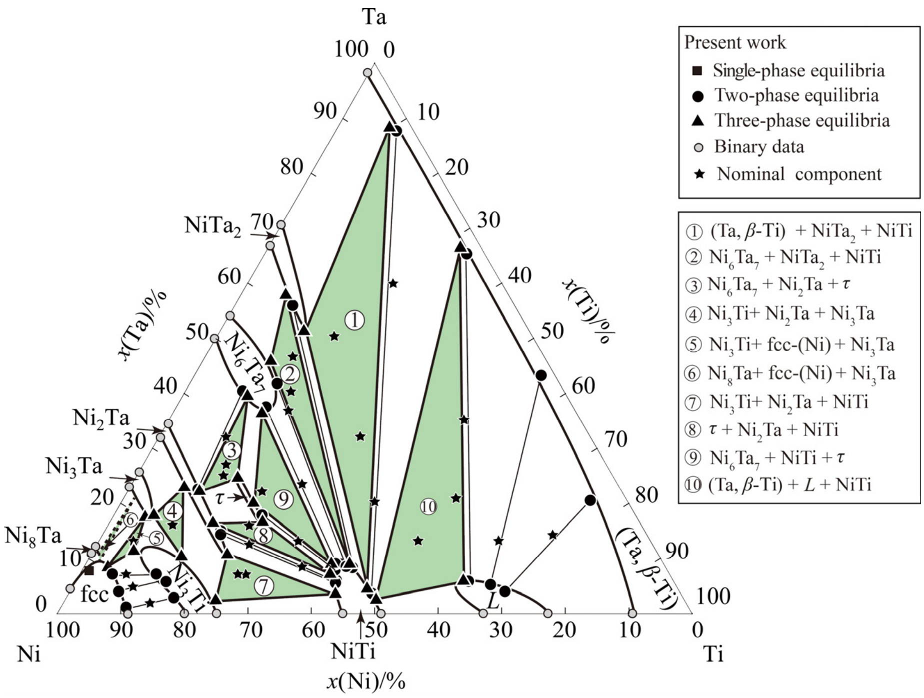

Fig. 6 Experimentally determined isothermal section of Ni−Ti−Ta system at 1000 °C

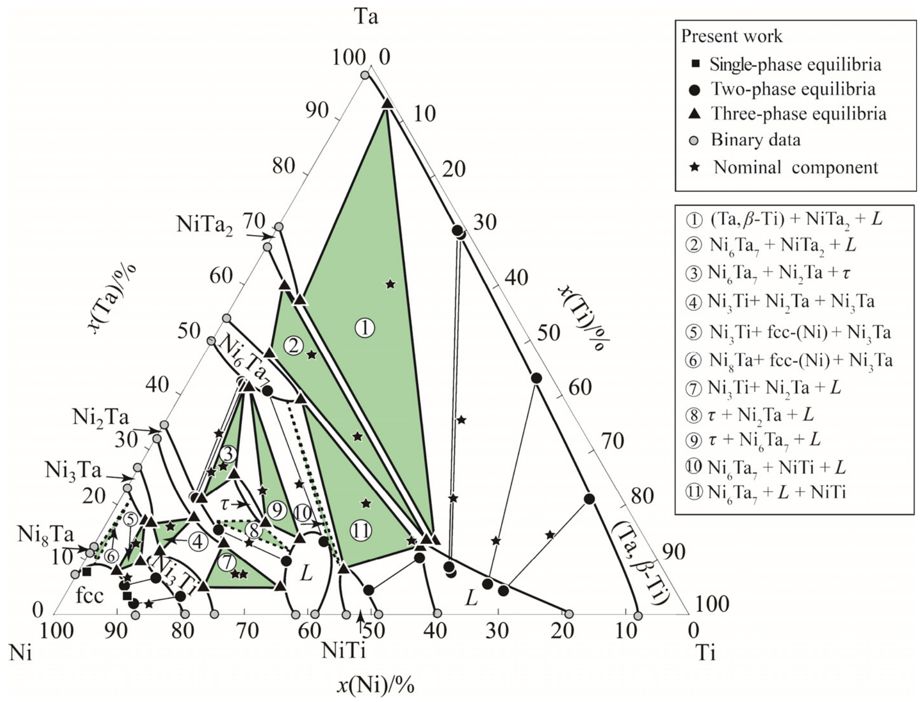

Fig. 7 Experimentally determined isothermal section of Ni−Ti−Ta system at 1200 °C

(Ta, β-Ti). The solubilities of Ta in the fcc-(Ni), Ni_3Ti and NiTi phases were about 9.0 at.%, 12.0 at.% and 9.7 at.%, respectively. Meanwhile, the Ni_3Ta, Ni_2Ta, Ni_6Ta_7 and $NiTa_2$ were dissolved at about 6.1 at.%, 21.9 at.%, 14.6 at.% and 13.5 at.% Ti, respectively.

Eight three-phase regions, ((Ta, β-Ti) + $NiTa_2$ + L), (Ni_6Ta_7 + $NiTa_2$ + L), (Ni_6Ta_7 + Ni_2Ta + τ), (Ni_3Ti + Ni_2Ta + Ni_3Ta), (Ni_3Ti + fcc-(Ni) + Ni_3Ta), (Ni_3Ti + Ni_2Ta + L), (τ + Ni_6Ta_7 + L) and (Ni_6Ta_7 + NiTi + L), were determined in the isothermal section of the Ni−Ti−Ta ternary system at 1200 °C. However, the remaining three three-phase equilibria of (Ni_8Ta + fcc-(Ni) + Ni_3Ta), (τ + Ni_2Ta + L)

and (Ni_6Ta_7 + NiTi + L) were inferred. The experimental results show that the ternary compound τ phase with almost the same composition range still existed at 1200 °C. Besides, with increasing temperature, a liquid phase presented within (38−41) at.% Ti.

4 Conclusions

(1) The isothermal sections of the Ni−Ti−Ta ternary system at 1000 and 1200 °C in the full composition range were experimentally established. Ten and eleven three-phase equilibria exist in this ternary system at 1000 and 1200 °C, respectively.

(2) A ternary compound τ phase with almost the same small solubility was determined at both temperatures. The composition ranges of τ phase were (58.5−60.0) at.% Ni, (15.9−24.1) at.% Ti and (16.3−22.4) at.% Ta at 1000 °C.

(3) The homogeneity ranges of binary compounds were measured and the phase relations among them were determined. The solid solubilities of Ti in Ni−Ta binary compounds and of Ta in Ni−Ti binary compounds were not large, but Ni_2Ta dissolved at 21.9 at.% Ti at 1000 °C.

Acknowledgments

This work was financially supported by the National Natural Science Foundation of China (No. 51831007), and National Key R&D Program of China (No. 2017YFB0702901).

References

[1] CARON P, KHAN T. Evolution of Ni-based superalloys for single crystal gas turbine blade applications [J]. Aerospace Science and Technology, 1999, 3: 513−523.

[2] POLLOCK T M, TIN S. Nickel-based superalloys for advanced turbine engines: Chemistry, microstructure and properties [J]. Journal of Propulsion and Power, 2006, 22: 361−374.

[3] BARRETT C A, MINER R V, HULL D R. The effects of Cr, Al, Ti, Mo, W, Ta, and Cb on the cyclic oxidation behavior of cast Ni-base superalloys at 1100 and 1150 °C [J]. Oxidation of Metals, 1983, 20: 255−278.

[4] YANG S W. Effect of Ti and Ta on the oxidation of a complex superalloys [J]. Oxidation of Metals, 1981, 15: 375−397.

[5] ZHANG H W, QIN X Z, WU Y S, ZHOU L I, LI X W. Effects of Cr content on the microstructure and stress rupture property of a directionally solidified Ni-based superalloy during long-term thermal exposure [J]. Materials Science and Engineering A, 2018, 718: 449−460.

[6] JANOWSKI G M, HECKEL R W, PLETKA B J. The effects of tantalum on the microstructure of two polycrystalline nickel-base superalloys: B-1900 + Hf and MAR-M247 [J]. Metallurgical Transactions A, 1986, 30: 1362−1365.

[7] NATHAL M V, EBERT L J. The influence of cobalt, tantalum, and tungsten on the elevated temperature mechanical properties of single crystal nickel-base superalloys [J]. Metallurgical Transactions A, 1985, 16: 1863−1870.

[8] COLLIER J P, KEEFE P W, TIEN J K. The effects of replacing the refractory elements W, Nb, and Ta with Mo in nickel-base superalloys on microstructural, microchemistry, and mechanical properties [J]. Metallurgical Transactions A, 1986, 17: 651−661.

[9] CHANG J X, WANG D, LIU T, ZHANG G, LOU L H, ZHANG J. Role of tantalum in the hot corrosion of a Ni-base single crystal superalloy [J]. Corrosion Science, 2015, 98: 585−591.

[10] HAN F F, CHANG J X, LI H, LOU L H, ZHANG J. Influence of Ta content on hot corrosion behaviour of a directionally solidified nickel base superalloy [J]. Journal of Alloys and Compounds, 2015, 619: 102−108.

[11] YAMASHITA M, KAKEHI K. Tension/compression asymmetry in yield and creep strengths of Ni-based superalloy with a high amount of tantalum [J]. Scripta Materialia, 2006, 55: 139−142.

[12] RAE C M F, REED R C. The precipitation of topologically close-packed phases in rhenium-containing superalloys [J]. Acta Materialia, 2001, 49: 4113−4125.

[13] SATO A, HARADA H, YOKOAWA T. The effects of ruthenium on the phase stability of fourth generation Ni-base single crystal superalloys [J]. Scripta Materialia, 2006, 54: 1679−1684.

[14] ZHOU C Y, GUO C P, LI C R, DU Z M. Thermodynamic optimization of the Ni−Ta system supported by the key experiments [J]. Thermochimica Acta, 2018, 666: 135−147.

[15] KEYZER J, CACCIAMANI G, DUPIN N, WOLLANTS P. Thermodynamic modeling and optimization of the Fe−Ni−Ti system [J]. Calphad, 2009, 33: 109−123.

[16] MURRAY J L. The Ta−Ti (tantalum−titanium) system [J]. Bulletin of Alloy Phase Diagrams, 1981, 2: 62−66.

[17] KAUFMAN L. Coupled thermochemical and phase diagram data for tantalum based binary alloys [J]. Calphad, 1991, 15: 243−259.

[18] ANSARA I, SELLEBY M. Thermodynamic analysis of the Ni−Ta system [J]. Calphad, 1994, 18: 99−107.

[19] PAN X M, JIN Z P. Experimental determination and Re-optimization of Ni−Ta binary system [J]. Transactions of Nonferrous Metals Society of China, 2002, 12: 748−753.

[20] LARSON J M, TAGGART R, POLONIS D H. Ni_8Ta in nickel-rich Ni−Ta alloys [J]. Metallurgical and Materials Transactions B, 1970, 1: 485−489.

[21] NASH P, WEST D R F. Ni−Al and Ni−Ta phase diagrams [J]. Metal Science, 1983, 17: 99−100.

[22] ZHOU Yi, WEN Bin, MA Yun-qing, MELNIK R, LIU Xing-jun. First-principles studies of Ni−Ta intermetallic compounds [J]. Journal of Solid State Chemistry, 2012, 187: 211−218.

[23] CUI Y W, JIN Z P. Experimental study and reassessment of the Ni−Ta binary system [J]. Zeitschrift fur Metallkunde, 1999, 90: 233−241.
[24] KAUFMAN L, NESOR H. Coupled phase diagrams and thermochemical data for transition metal binary systems—I [J]. Calphad, 1978, 2: 55−80.
[25] MICHAL G M, SINCLAIR R. The structure of TiNi martensite [J]. Acta Crystallographica: Section B, 1981, 37: 1803−1807.
[26] POVODEN-KARADENIZ E, CIRSTEA D C, LANG P, WOJCIK T, KOZESCHNIK E. Thermodynamics of Ti−Ni shape memory alloys [J]. Calphad, 2013, 41: 128−139.
[27] HU Biao, DU Yong, SCHUSTER J C, SUN Wei-hua, LIU Shu-hong, TANG Cheng-ying. Thermodynamic modeling of the Cr−Ni−Ti system using a four-sublattice model for ordered/disordered bcc phases [J]. Thermochimica Acta, 2014, 578: 35−42.
[28] SANTHY K, HARI KUMAR K C. Thermodynamic reassessment of Nb−Ni−Ti system with order–disorder model [J]. Journal of Alloys and Compounds, 2015, 619: 733−747.
[29] GUPTA K P. The Ni−Ta−Ti (nickel−tantalum−titanium) system [J]. Phase Diagram of Ternary Nickel Alloys, 1991, 2: 203−207.
[30] DU Yong, XU Hong-hui, ZHOU Yi-chun, OUYANG Yi-fang, JIN Zhan-peng. Phase equilibria of the Ni−Ti−Ta system at 927 °C [J]. Materials Science and Engineering A, 2007, 448: 210−215.

Ni−Ti−Ta 三元体系的相平衡关系

王翠萍[1]，杨 鹏[1]，梁宇辉[1]，杨水源[1]，韩佳甲[1]，卢 勇[1]，刘兴军[1,2,3]

1. 厦门大学 材料学院 福建省材料基因组重点实验室，厦门 361005；
2. 哈尔滨工业大学 先进焊接与连接国家重点实验室，哈尔滨 150001；
3. 哈尔滨工业大学 材料基因组与大数据研究所，深圳 518055

摘 要：采用 X 射线衍射和电子探针显微分析方法，获得 Ni−Ti−Ta 三元体系在 1000 和 1200 ℃的全成分范围内等温截面相图。实验结果显示，Ni−Ti−Ta 三元体系的 1000 和 1200 ℃等温截面相图中均存在一个固溶度较小的三元化合物 τ 相，且通过相平衡可知，该相在 1000 ℃的成分为(16.3~22.4)% Ta，(15.9~24.1)% Ti 和(58.5~60.0)% Ni(摩尔分数)。此外，在这两个等温截面相图中，bcc-(Ta)和 β-Ti 均形成连续的固溶体。Ti 在 NiTa 二元化合物中均有一定的固溶度，其中，1000 ℃时 Ti 在 Ni_2Ta 中的固溶度达 21.9%(摩尔分数)。

关键词：显微组织；Ni−Ti−Ta 三元体系；等温截面相图；电子探针显微分析

(Edited by Wei-ping CHEN)